Conference Paper, Published Version

Cheng, Liang; Zhao, Ming; Li, F.; An, H. W.

Numerical model for wave-induced scour below a piggyback pipeline

Numerical model for wave-induced scour below a piggyback pipeline

L. Cheng[1], M. Zhao[1], F. Li[2] and H.W. An[1]
[1] School of Civil and Resource Engineering, The University of Western Australia, 35 Striling Highway, Crawley, WA 6009, Australia
[2] CSIRO Petroleum, 26 Dick Perry Ave, Kensington, WA 6151,Australia

Local scour below a piggyback pipeline due to wave action is investigated numerically. The piggyback pipeline consists of two pipelines of different diameters with the small one being located directly at the top of the large one (as shown in Fig. 1). Wave-induced flow around the pipeline is assumed to be sinusoidal oscillatory flow. The Reynolds averaged Navier-Stokes equations and the *k-ω* turbulent equations are solved using a finite element method. The conservation of the sediment mass is solved for predicting the bed scour profile. The model is firstly validated against the scour below a single pipeline under waves, where the experimental data are available. Then the model is employed to simulate the scour below a piggyback pipeline in waves. Computations are carried out for the diameter ratio of the small pipe diameter (*d*) to the larger one (*D*) equal 0.2 and the KC number, based on the large pipeline diameter, equals 12. The gap between the two pipelines ranges from 0.05*D* to 0.5*D*. The effects of the gap ratio *G*/*D* on the scoured bed profile are investigated numerically.

I. INTRODUCTION

Scour below a pipeline in currents has been investigated both experimentally and numerically in the past decades. It is well understood that the scour hole behind the pipeline is much gentler than that in front of the pipeline. The experiments showed that the scour can be classified into two stages [1, 2]. In the early stage of the scour development there is no vortex shedding behind the pipeline. The jet flow through the gap between the pipeline and the bed plays an important role in the scour process. This is called tunnel scouring [2]. As the scour depth under the pipe increases to a certain value and the gap between the pipe and bed becomes large enough, the vortex shedding occurs. The vortex shedding dominates the scour process from this moment onwards. This type of scour is called lee-wake scour [2].

Numerical models were also established for simulating the local scour below pipelines in currents in the past. It had been demonstrated that the models based on the potential flow can not predict the vortex shedding induced gentle slope behind the pipe [3, 4]. The turbulent flow model is mainly used in recent years to resolve the flow field in the scour models. Several scour models based on the turbulence model were established [4-7].

Investigations of scour below pipelines in waves are rarer than in currents. Sumer and Fredsøe [8] investigated the scour below pipelines in waves by physical experiments. They found that the scour process is mainly governed by the Keulegan-Carpenter (KC) number. The KC parameter is defined by $KC=U_mT/D$, where U_m is the velocity amplitude of the oscillatory flow, T is the period of the flow and D is the pipeline diameter. Liang and Cheng [9] simulated the scour below pipelines in waves numerically using a finite difference method (FDM). They found that the steady streaming always exists and directs away from the pipeline.

In this study, a finite element model (FEM) is established for simulating the scour below a piggyback pipeline in waves. It is expected that the FEM model offers more flexibility in handling the irregular computational domain created by local scour of the seabed. In the present model, the flow is simulated by solving the Navier-Stokes equations. The k-ω model is applied to simulate the turbulence of the flow. The sediment transport rates (includes bed load and suspended load) are calculated. The bed profile evolution is predicted by solving the conservation equation of the sediment mass. The model is firstly validated against wave scour below a single pipeline. The computed scour profiles are compared with the experimental data. Then the scour model is applied to simulate the scour below a piggyback pipeline under wave action. The piggyback pipeline consists of two pipelines of different diameters with the small one is located directly at the top of the large one (as shown in Fig. 1). Computations are carried out for the diameter ratio of the small pipe diameter (d) to the larger one (D) equal 0.2 and KC number based on the large pipeline diameter equal 12. The gap between the two pipelines ranges from 0.05D to 0.5D.

II. NUMERICAL METHOD

Local scour below a piggyback pipeline in waves (as shown in Fig. 1) is considered. The piggyback pipeline consists of two pipelines of different diameters. The small pipe is placed on top of the large one. The large pipeline is initially mounted on the sandy sea bed. In this study, the wave motion is assumed to be sinusoidal oscillatory flow [9]. The numerical model comprises of a flow model, a sediment transport model and a morphological model.

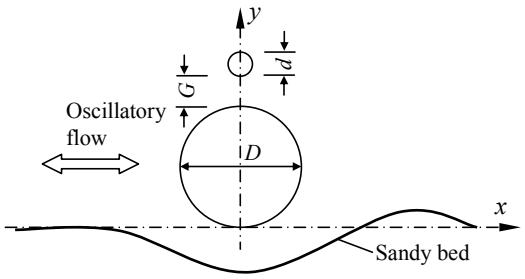

Fig. 1 Sketch of flow wave scour below a piggyback pipeline

The flow is simulated by solving a set of Reynolds-averaged Navier-Stokes equations. The turbulence of the flow is simulated by the *k-ω* turbulent model. The Reynolds-averaged Naiver-Stokes equations and the *k-ω* equations are solved by the finite element model proposed by Zhao et al. [10]. The details on the model can be found in reference [10].

A rectangular computational domain is employed in the computation. The pipeline is placed at the center of the domain. At the left and right boundaries, the vertical velocity component is set to be zero, and the profiles for the horizontal velocity, turbulent quantities are obtained based on the equilibrium profiles obtained from a separate calculation of oscillatory flow in a channel with a flat bed using the same program. Pressure at the right boundary is given a reference value of zero. At the upper boundary, vertical velocity component is set to be zero and zero normal gradient condition is applied to the turbulent quantities and pressure. On the wall boundaries, the standard wall function boundary condition is implemented [5].

The transport of sediment particles by a flow are generally in the form of bed-load and suspended load. The bed-load is the transport of sediment particles in a thin layer of about 2 sediment particle diameters thick above the bed by sliding, rolling and sometimes jumping with a longitudinal distance of a few particle diameters [11]. In this paper the bed load transport rate is calculated by the following equation proposed by Engelund and Fredsøe [12]:

$$q_b = \frac{1}{6}\pi d_{50}^3 d P_{EF} U_b \tag{1}$$

where d_{50} is the median grain diameter, P_{EF} is the percentage of particles in motion in the surface layer of the bed, U_{b} is the mean transport velocity of a particle moving along the bed. The U_{b} and P_{EF} are calculated by the following empirical formulae [12]:

$$U_b = a u_f (1 - 0.7\sqrt{\theta / \theta_c}) \tag{2}$$

$$P_{EF} = \left[1 + \left(\frac{1}{6}\frac{\pi\mu_d}{\theta - \theta_c}\right)^4\right]^{1/4} \tag{3}$$

where $u_f = \sqrt{\tau/\rho}$ is the friction velocity, τ is the bed shear stress, $a = 10$ is an experimental constant, $\theta = u_f^2/[g(s-1)d_{50}]$ is the Shields parameter, θ_c the threshold Shields parameter, μ_d is the dynamic friction coefficient, taken as 0.51 [13]. For sand on a slope bed, the threshold Shields parameter is modified as [14] $\theta_c = \theta_{c0}(\cos\alpha + \sin\alpha/\tan\phi)$, where θ_{c0} is the threshold Shields parameter on a flat bed, α is the bed slope angle, ϕ is the angle of repose of the sediment.

The suspended load transport rate is calculated according to the suspended sediment concentration. The volumetric concentration *c* of the suspended sediment is calculated by solving the following transport equation.

$$\frac{\partial c}{\partial t} + u_1\frac{\partial c}{\partial x_1} + (u_2 - w_s)\frac{\partial c}{\partial x_2} = \frac{\partial}{\partial x_j}\left(\frac{\nu_t}{\sigma_c}\frac{\partial c}{\partial x_j}\right) \tag{4}$$

where w_{s} is the settling velocity of the sediment in the water, σ_c is the turbulent Schmidt number which is taken to be 0.8 in present study. The settling velocity in clear water w_{s0} is computed by [15]:

$$w_{s0} = (\nu/d_{50})[(10.36^2 + 1.049D_*^3)^{1/2} - 10.36] \tag{5}$$

In order to consider the reduction of the settling velocity due to the interaction of the sediment grains, the w_{s} is modified by [16] $w_s = w_{s0}(1-c)^m$, where *m* is a constant which is set to be 5. The sediment concentration at the interface of the bed load and the suspended load, which is $2d_{50}$ above the wall, is specified based on the experimental formula [17]

$$c_a = [0.331(\theta - 0.045)^{1.75}]/[1 + 0.72(\theta - 0.045)^{1.75}] \tag{6}$$

Following Zyserman and Fredsøe [17], the threshold Shields parameter for computing the reference concentration is set to be 0.045 as shown in Eq. (10). If the bed Shields parameter is smaller than the threshold Shields parameter, the zero normal gradient of the sediment concentration is applied [6]. Eq. (5) is also solved by a finite element method in a same mesh of the flow calculation.

The suspended transport rate (q_s) is calculated by $q_s = \int_{z_b+\Delta_b}^{z_s} u_1 c dz$, where z_{s} is the water surface level, $\Delta_b = 2d_{50}$ is the reference level below which the sediment is transported as the bed load and above which the sediment transported as suspended load.

The time averaged bed load ($\overline{q}_s$) and suspended load ($\overline{q}_b$) is calculated by averaging them over a wave period. The following conservation equation of the sediment mass is solved for modeling the bed profile evolution.

$$\frac{\partial z_b}{\partial t} = -\frac{1}{1-\lambda}\frac{\partial}{\partial x}(\overline{q}_b + \overline{q}_s) \tag{7}$$

where z_b is the bed elevation, λ is the sediment porosity.

In scour calculations, the computational mesh needs to be updated in each morphological time step. After the bed level is updated, the nodal points of the mesh are adjusted according to the updated bed profile. In this study, the fluid domain is considered as an imaginary elastic solid [18] when updating the mesh. The displacement of the mesh is governed by the equilibrium equations of elasticity by specifying the displacement along the bed. In order to avoid excessive deformations of small size elements, variable Lame elastic constants of the elastic solid are applied to elements to provide more

stiffness to small elements [18].

The computational procedure can be summarized as follows:

(1) Solve the Reynolds-averaged Navier-Stokes equations, the turbulent equations and the convection-diffusion equation of the sediment concentration. If the flow calculation reaches the equilibrium state (the flow velocity, the turbulent quantities and the sediment concentration in two successive periods are almost same), the scour computation is started.

(2) Calculate the bed load and the suspended load in one wave period, while solving the flow and turbulent equations.

(3) Average the bed load and the suspended load over one wave period to obtain the time averaged transport rates.

(4) Calculate the bed profile at next morphological time step according to Eq. (7). The morphological time step is selected to be much larger than the flow time step in order to speed up the calculation.

(5) Sand-slide model [5] is applied to guarantee the slope angle of the bed is not larger than the repose angle of the sediment grain.

(6) Update the mesh according to the updated bed profile.

(7) Keep bed profile constant and solve the flow equations for a number of wave periods to allow the equilibrium state being reached after the bed change.

(8) Iterate from step (2) to (7) until the bed change rate approaches to zero.

III. WAVE SCOUR BELOW A SINGLE PIPELINE

The scour model is firstly applied to simulate the local scour below a single pipeline in waves in order to validate the model. The wave motion is modeled by a sinusoidal oscillatory flow [4]. The scour process for KC = 7 in the experiments of Sumer and Fredsøe [8] is simulated. In order to make a direct comparison with the experimental results, the computation is carried out under the conditions which are the same as those specified in the physical experiment [8]. In the experiment, the pipeline diameter was 0.05 m. The amplitude of the oscillatory flow is 0.228 m/s. The median sediment grain size was d_{50} = 0.58 mm. The Reynolds number is 1.1×10^4. In the present computation, the pipeline diameter and the sediment grain size are selected to be same as those used in the experiment. A computational domain of a width of 60D and a height of 6D is used. The pipeline is located at the middle cross-section of the domain. The depth-averaged velocity amplitude is 0.228 m/s.

The pipeline is originally placed on a flat sandy bed. Fig. 2 shows the initial computational mesh near the pipe. An initial scour hole of a depth of 0.1D beneath the pipeline is introduced to avoid a complete re-meshing during the calculation. It has been demonstrated in early studies that the introduction of the initial scour hole has negligible effect on the modeled subsequent scour developments [5]. Fine structural quadrilateral elements are employed near the pipeline surface and the bed. The pipeline surface is discretized using 120 nodes. The total number of nodal points in the mesh shown in Fig. 2 is 18534.

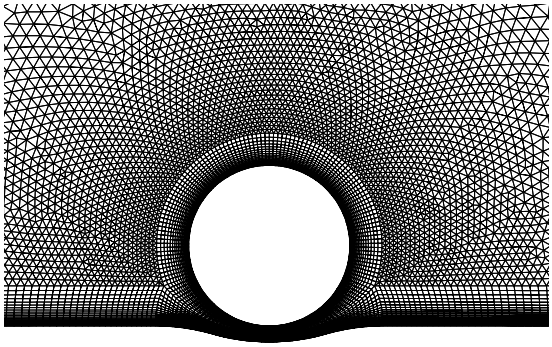

Fig. 2 Initial computational mesh for a single pipeline

Fig. 3 shows the comparison of the bed profiles at three instants after the initiation of the scour. The computed results agree well with the experimental data [8]. Two small sand dunes form at the beginning of the scour. These two dunes are transported away from the pipeline and their heights decrease with time. At t = 55 min, the scour rate approaches to zero. In the early stage of the scour, both the measured and the computed bed profiles are almost symmetric with respect to the pipeline center. The measured bed profile becomes asymmetric at the equilibrium state (See Fig. 3 (c)). However, the computed bed profile keeps symmetric throughout the duration of the scour. The asymmetry of the bed profile observed in the experiment likely attributes to the fact that the oscillation of the wave particle velocity in the experiment is not exactly sinusoidal due to the nonlinearity.

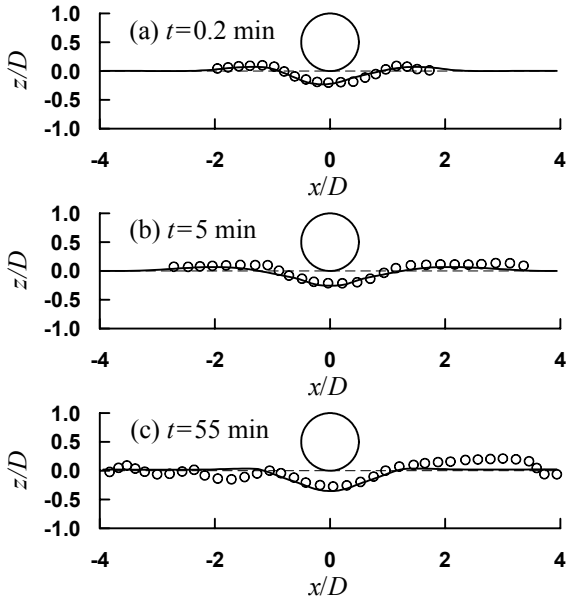

Fig. 3 Comparison of the bed profiles. ○○○, experimental [8]; ——, numerical

Fig. 4 shows the distribution of the period averaged bed load and suspended load sediment transport rates. It is seen that the directions of the sediment transport rates are away from the pipeline. The high transport rate occurs in the vicinity of the pipeline. The period averaged sediment transport rates far away from the pipeline approach to zero because the effect of the pipeline on the flow is weak. The bed load transport rate is much larger than the suspended load transport rate in the study case. Both bed load and suspended load transport rates decrease with time. At $t = 55$ minutes, the variation of the sediment transport rate with x is rather weak. It is also observed that the variation of the bed profile with time approaches to zero at $t = 55$ minutes.

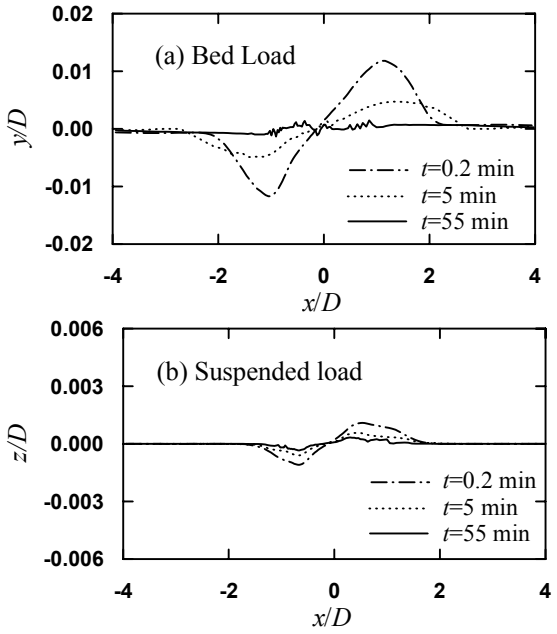

Fig. 4 Distribution of the period averaged sediment transports

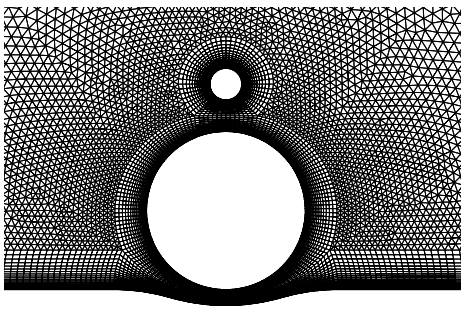

Fig. 5 Finite element mesh for $G/D = 0.2$

IV. WAVE SCOUR BELOW A PIGGYBACK PIPELINE

The finite element model is applied to simulate the wave-induced scour below a piggyback pipeline. The piggyback pipeline comprises of two pipelines of different diameters as shown in Fig. 1. The large pipeline diameter is 0.25 m. The diameter ratio d/D is kept to be 0.2. The gap between the small pipeline and the large one is G. The sediment grain diameter is $d_{50} = 0.5$ mm. The wave is modeled by sinusoidal oscillatory flow. The wave period is 6 s. The amplitude of the depth averaged velocity (U_m) is 0.5 m/s. The KC number and the Reynolds number (both based on the large pipeline diameter) are 12 and 1.25×10^5 respectively. The computational domain with a depth of $6D$ and a width of $30D$ is divided into un-structured finite elements. Fig. 5 is an example of the finite element mesh in the vicinity of the pipeline for $G/D = 0.2$. Computations are carried out for $G/D = 0.1$, 0.15, 0.2, 0.3, 0.4 and 0.5. The effect of G/D on the scour depth is investigated numerically.

Computations are carried out until two hours after scour. Fig. 6 shows the comparison of the time history of the scour depth just below the large pipeline centre (S_0). The S_0 in the single large pipeline case is also plotted in Fig. 6 for comparison. It can be seen from Fig. 6 that the scour rate at the beginning of the scour is very large, it decreases with time. At the moment of $t = 2$ hours, the scour rate for all cases has become very small. It is seen that the scour depths at $GD = 0.15$ and 0.20 are larger than that of the single pipeline case. The scour rate for $G/D = 0.10$ is close to those for $GD = 0.15$ and 0.20 before $t = 1$ hour. After $t = 1$ hour the scour rate for $G/D = 0.10$ is almost zero. At the S_0 for $G/D = 0.30$, 0.40 and 0.50 approaches to that in single pipeline case. It is expected that the effect of the small pipeline on the large one becomes weak in these two cases.

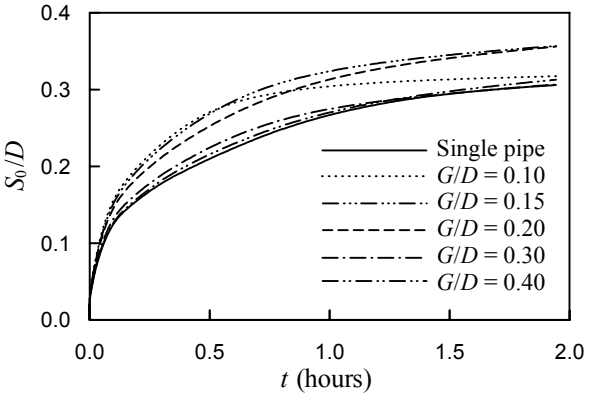

Fig. 6 Time histories of the scour depth just below the pipeline center

Fig. 7 shows the variation of the scour depth below the pipeline center versus G/D ratio at $t = 2$ hours. The scour depth in Fig. 7 is normalized by that of single pipeline (S_{01}) case. It is seen that at $G/D = 0.15$ and 0.20 the scour depth is about 1.17 times of that in single pipeline case.

For all different G/D cases, two sand dunes forms at the two sides of the pipeline after the onset of the scour. The sand dunes move away from the pipeline and their heights decreases with time. Fig. 8 shows the scour profiles at $t = 2$ hours for different values of G/D. It is seen from Fig. 8 that the bed shape is similar to that in single pipeline case except the case of $G/D = 0.10$. For $G/D = 0.10$, the two sand dunes are still not far way from the pipeline. It is found that the sand dunes are still moving away from the pipeline at a very slow speed. But the scour depth below the pipeline center for $G/D = 0.10$ has reached a constant at $t = 2$ hours (as shown in Fig. 6).

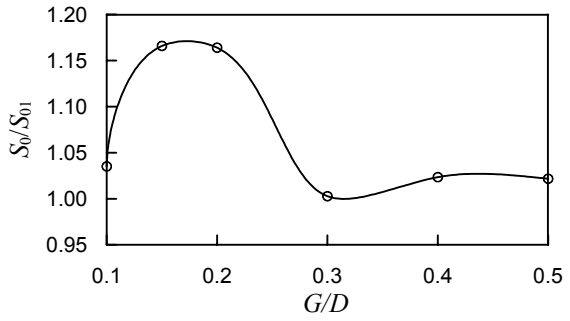

Fig. 7 Variation of scour depth below pipeline center versus G/D (t = 2 hours)

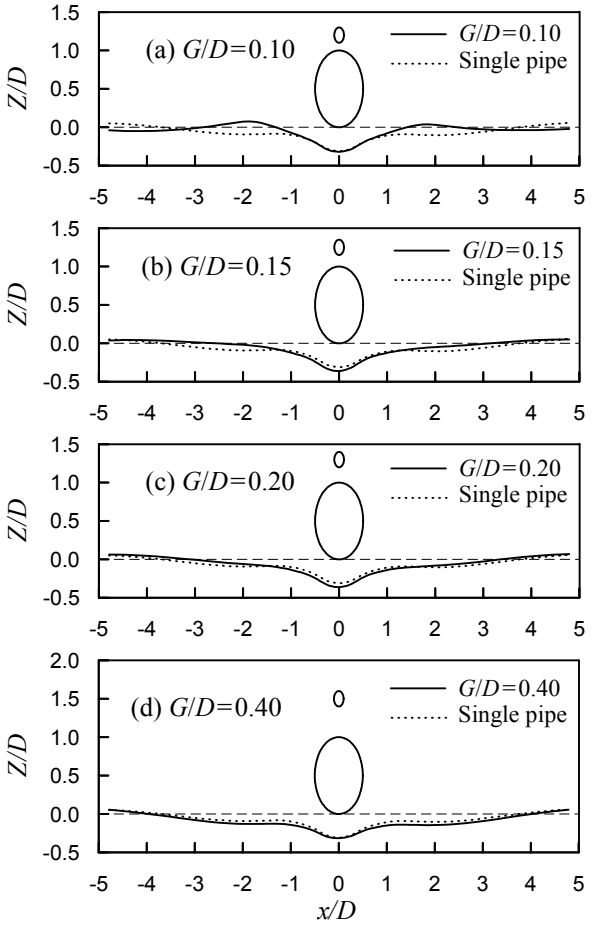

Fig. 8 Scour profiles for different values of G/D (t = 2 h)

The gentle slopes of the scour hole at both sides of the pipeline in Fig. 8 are similar to lee-wake induced scour in steady current case. Mao [1] had demonstrated that the gentle slope in the wake of the pipeline is due to the vortex shedding. Zhao and Cheng [7] also reproduced the lee-wake scour process by numerical method. In case of wave scour, the vortex shedding occurring in each half of wave period is similar to that in the steady current case. If the KC number is large, more vortices will be shed from the pipeline in a half of a period. The larger the KC number is, the further away from the pipelines they will be transported. It is expected that the increase of KC number will lead to gentler slopes of the scour hole at both sides of the pipelines. It can be demonstrated by comparing the scour hole at lower KC in Fig. 8 with that studied in Section III (Fig. 3).

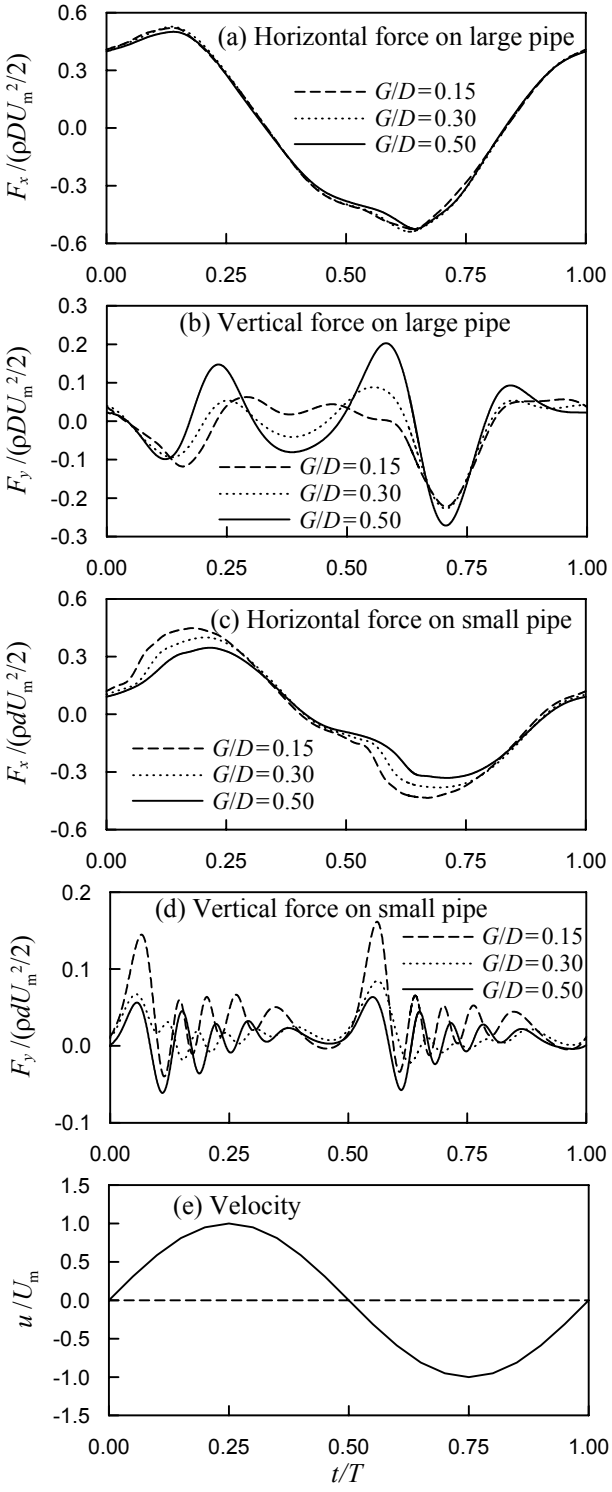

Fig. 9 Time histories of the hydrodynamic forces on the pipelines

Fig. 9 shows the time history of the hydraulic force on the large and the small pipelines after t = 2 hours. The t/T = 0 instant in Fig. 9 corresponds to t = 2 hours. T is wave period. It can be seen that effect of the gap ratio (G/D) on the hydraulic force is significant. The amplitudes of the fluctuating in-line forces on both large pipeline and the

small pipeline decrease with the increase of G/D. The decrease rate of the large pipeline is much smaller than that of the small pipeline. It is seen from Fig. 9 (a) and (c) that the maximum in-line forces reach their maximum values prior to the velocity. The phase shift between the maximum in-line force and the maximum velocity is about 30 degree.

The fluctuation of the lift force on the pipelines is due to the flow reverse and the vortex shedding [19]. The frequency of the lift force on the small pipeline is much larger than that on the large pipeline. The KC number based on the small pipeline is 60, which is 5 times that based on the large pipeline. It is observed that the number of vortices shed from the small pipeline in one wave period is much more than the number shed from the large pipeline. The frequency of the lift force on the large pipeline is about three times of the wave frequency. The frequency of the lift on the small pipeline is ten times of the flow frequency.

The drag and inertia coefficient on each pipeline is obtained by fitting the computed in-line force with the Morison equation using the least square method. The Morison equation is

$$F_x = \frac{1}{4}\rho\pi D^2 C_M \frac{du}{dt} + \frac{1}{2}\rho D C_D u|u| \qquad (8)$$

where C_D and C_M are the drag and inertia coefficients respectively. The drag and inertia coefficients on the small pipeline are also calculated by Eq. (8) based on the small pipeline diameter. Two lift coefficients are examined. The lift coefficients C_{L+} and C_{L-} on the large pipeline are defined as

$$C_{L+} = \max(F_y / \rho D U_m^2 / 2) \qquad (9)$$

$$C_{L-} = \min(F_y / \rho D U_m^2 / 2) \qquad (10)$$

The lift coefficients C_{L+} and C_{L-} on the small pipeline are also calculated by Eqs. (9) and (10) by replacing D with d.

Fig. 10 shows the variation of the force coefficients versus G/D after 2 hours of scour. Both the drag coefficient and the inertia coefficient on the large pipeline are smaller than their counterparts on the small pipeline. This is because that part of the large pipeline is immerged in the boundary layer of the flow in which the flow velocity is very small. The effects of G/D on C_D and C_M of large pipeline are weaker than those of small pipeline. The C_D and C_M on the small pipeline decreases with the increase of G/D. The C_D on the large pipeline changes little with G/D except a slight decrease as G/D increase from 0.1 to 0.15. The C_M on the large pipeline does not change with G/D either.

The C_{L+} on the large pipeline increases with the increase of G/D but decreases with the increase of G/D on the small pipeline. The change rates of the C_{L-} on both pipelines are small relative to those of C_{L+}. The vector of average lift coefficient ($\overline{C}_L = (C_{L+} + C_{L-})/2$) is away from bed and that on the large pipeline is towards the bed when G/D is small. It approaches zero at $G/D > 0.40$. It can be seen From Fig. 10 (c) that the absolute value C_{L-} is almost the same as C_{L+} with $G/D = 0.50$ for both pipelines. The symmetry of the lift coefficients can also be found in Fig. 9 (d). The symmetry is because the interaction between the two pipelines becomes weak at large value of G/D.

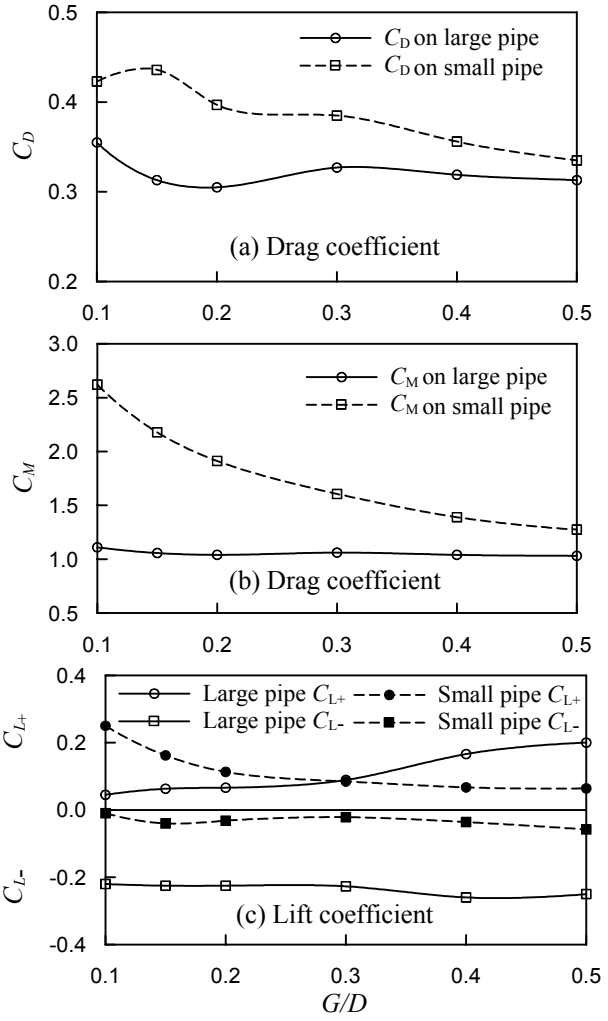

Fig. 10 Variation of the force coefficient versus G/D ($t = 2$ h)

CONCLUSIONS

The wave-induced scour below a piggyback pipeline is investigated numerically. The vertical two-dimensional finite element model is established for simulating the scour. The turbulent flow is simulated by solving the Reynolds-averaged Navier-Stokes equations with the k-ω turbulent model. The bed evolution is updated by solving the sediment mass conservation equation. In order to speed up the computational speed the morphological time step is selected to be much larger than the flow time step. The model is firstly used to simulate the scour below a single pipeline under waves. The pipeline is initially placed on a flat sandy bed. The wave motion is modeled by a sinusoidal oscillatory flow. The predicted scour holes agree well with Sumer and Fredsøe [8] experimental results (KC=7 case).

The scour below a piggyback pipeline is then investigated. The calculations are carried out for KC=12 and the gap ratio G/D ranging from 0.1 to 0.5. It is found that the maximum scour depth just below the pipeline occurs in the intermediate gap ratio $G/D = 0.15$ and 0.20. The scour profiles for $G/D \geq 0.30$ are similar to those of

the single pipeline case. The KC number affects the slope of the scour hole. The slope is steep for small KC number and gentle for large KC number.

The force coefficients on the pipelines above the scoured bed are also studied. The effect of the gap on the force on the small pipeline is much stronger than that on the large pipeline. The C_D and C_M on the small pipeline decrease with the increase of G/D. The change rates of the C_{L-} on both pipelines are small relative to those of C_{L+}. The averaged lift coefficient $\overline{C}_L$ is away from the bed and that on the large pipeline is towards the bed when G/D is small. It approaches zero when $G/D > 0.40$.

ACKNOWLEDGMENT

The authors would like to acknowledge the supports from Australia Research Council through ARC Discovery Projects Program Grant No. DP0557060.

REFERENCES

[1]. Mao, Y., 1986, The interaction between a pipeline and an erodible bed, Ser. Paper 39, Institute of Hydrodynamics and Hydraulic Engineering, Technical University of Denmark, Lyngby, Denmark.

[2]. Sumer, B.M. and Fredsøe J., 2002, The mechanics of scour in the marine environment, World Scientific, pp 15 - 138.

[3]. Sumer, B.M., Jensen, H.R. and Fredsøe, J, 1988, Effect of lee-wake on scour below pipelines in current, J. Waterw. Port Coast. Ocean Eng., Vol 114, No 5, pp 599-614.

[4]. Li, F. and Cheng, L., 2001, Prediction of lee-wake scouring of pipelines in currents, J. Waterw. Port Coast. Ocean Eng. Vol 127, No 2, pp 106-112.

[5]. Liang, D., Cheng, L. and Li, F., 2005, Numerical modeling of flow and scour below a pipeline in currents Part II. Scour simulation, Coastal Eng. Vol 52, pp 43-62.

[6]. Brørs, B., 1999 Numerical modeling of flow and scour at pipelines, J. Hydraul. Eng, Vol 125, No 5, pp 511-523.

[7]. Zhao M. and Cheng L., 2006. Numerical modeling of local scour below a piggyback pipeline in currents. Submitted to Journal of Hydraulic Engineering.

[8]. Sumer, B.M. and Fredsøe J., 1990, Scour below pipelines in waves, J. Waterw. Port Coast. Ocean Eng., Vol 116, No 3, pp 307-323.

[9]. Liang, D., and Cheng, L., 2005, Numerical model for wave-induced scour below a submarine pipeline, J. Waterw. Port Coast. Ocean Eng. Vol 131, No 5, pp 193-202.

[10]. Zhao, M., Cheng, L., Teng, B., Dong, G., 2005, Hydrodynamic forces on dual cylinders of different diameters in steady currents, Submitted to Journal of Fluids and Structures.

[11]. Einstein, H.A., 1950, Bed-load function for sediment transportation in open channel flow, United States Department of Agriculture, Washington D.C., Technical Bulletin, No. 1026, pp. 25.

[12]. Engelund, F. and Fredsøe, J., 1976, A sediment transport model for straight alluvial channels, Nordic Hydrol., Vol. 7, pp. 293-306.

[13]. Fredsøe, J., Deigaard, R., 1992, Mechanics of Coastal Sediment Transport, Advanced Series on Ocean Engineering 3. Word Scientific, Singapore.

[14]. Allen, J. R. L., 1982, Simple models for the shape and symmetry of tidal sand waves: I. Statically stable equilibrium forms, Mar. Geol. Vol. 48, pp. 31-49.

[15]. Soulsby, R., 1997, Dynamics of Marine Sands. Tomas Telford, London.

[16]. Richardson, J.F., Zaki, W. N., 1954, Sedimentation and fluidisation: Part I, Trans. Inst. Chem. Eng., Vol. 32, No. 1, pp. 35-53.

[17]. Zyserman, J.A., Fredsøe, J., 1990, Data analysis of bed concentration of suspended sediment, J. Hydraulic Engineering, Vol. 120, No. 9, pp. 1021-1042.

[18]. Johnson, A.A., Tezduyar, T, E., 1994, Mesh update strategies in parallel finite element computations of flow problems with moving boundaries and interfaces, Comput. Methods Appl. Mech. Engrg, Vol. 119, pp. 73-94.

[19]. Williamson, C.H.K. 1985. Evolution of a single wake behind a pair of bluff bodies, Journal of Fluid Mechanics, 159, 1-18.